Characterization of Ni−Fe/MgO/Olivine Catalyst for Fluidized Bed Steam Gasification of Biomass

D. Świerczyński,[†] C. Courson,[†] L. Bedel,[†] A. Kiennemann,*[,†] and J. Guille[‡]

Laboratoire des Matériaux, Surfaces et Procédés pour la Catalyse − ECPM, UMR 7515 25, rue Becquerel, 67087 Strasbourg Cedex 2, France, and Groupe des Matériaux Inorganiques − IPCMS, UMR 7504 23 rue du Loess, 67037 Strasbourg Cedex, France

Received June 9, 2006

Tar removal catalyst development is the main hurdle to improving the process of steam biomass gasification in a fluidized bed. A Ni/olivine catalyst has been previously developed to enhance the catalytic properties of calcined natural olivine and showed excellent performance and stability during biomass steam gasification in the fast internally circulating fluidized bed (FICFB) gasifier. However, the origin of its active phase was not well-understood. The present work explains the mechanism of formation and the nature of the active phase of the Ni/olivine catalyst, characterized before testing, after calcination, and after reduction by means of X-ray diffraction (XRD), scanning electron microscopy (SEM), temperature-programmed reduction (TPR), and ^{57}Fe Mössbauer spectroscopy. Two phenomena contribute to the formation of this active system: the formation of a NiO−MgO solid solution on the olivine surface during calcination and Ni−Fe alloys during the reduction, both of which are known to have beneficial effects on increasing carbon deposition resistance. The catalyst, resulting from subsequent calcination and reduction of the precursor after the impregnation of natural olivine with nickel nitrate, can be described as a Ni−Fe/MgO/olivine system. Its catalytic performances are confirmed in the steam reforming of methane and toluene as a tar model compound.

Introduction

Biomass gasification in a fluidized bed permits the efficient production of syngas for chemical synthesis (biofuels, methanol, chemicals) or electricity production (hydrogen fuel cell, gas turbine, or engine), contributing to sustainable development and reduction of CO_2 emissions. The development of an appropriate catalyst for assisting in the removal of tars, light hydrocarbons, and ammonia and thus purifying the product gas and increasing syngas yield is one of the main challenges to improving and implementing gasification technology. Two solutions are possible for catalytic tar removal: primary treatments inside the gasifier or secondary treatment after the gasifier.[1] The optimal solution is using a catalyst as fluidized bed material, avoiding the expenses for additional secondary tar removal. The catalyst should then be active in reforming hydrocarbons and resistant to carbon deactivation as well as to attrition. Until now, different catalytic systems have been studied, including metal-based catalysts (Ni,[2−5] Fe,[6] Co,[7] Rh[8]), cheap minerals such as dolomites,[9−18] olivines,[11,19−22] or other oxides such as ZrO_2.[23] Nickel catalysts present the best activity/price compromise. However, deactivation by carbon formation and attrition is the main problem that needs to be solved before nickel catalysts can be used in a fluidized bed reactor.

In this study, we present the elaboration of a cheap nickel steam-reforming catalyst designed for the circulating fluidized bed gasifier, which, according to Bridgwater,[24] is the

* Corresponding author. Tel.: 33-390-2427-66. Fax: 33-390-2427-68. E-mail: kiennemann@chimie.u-strasbg.fr.

[†] ECPM.

[‡] IPCMS.

(1) Devi, L.; Ptasinski, K. J.; Janssen, F. J. J. G. *Biomass Bioenergy* **2003**, *24*, 125.
(2) Simell, P.; Kurkela, E.; Ståhlberg P.; Hepola, J. *Catal. Today* **1996**, *27*, 55.
(3) Bangala, D. N.; Abatzoglou, N.; Martin, J. P.; Chornet, E. *Ind. Eng. Chem. Res.* **1997**, *36* (10), 4184.
(4) Corella, J.; Orío, A.; Toledo, J. M. *Energy Fuels* **1999**, *13*, 702.
(5) Wang, T.; Chang, J.; Cui, X.; Zhang Q.; Fu, Y. *Fuel Process. Technol.* **2006**, *87* (5), 421.
(6) Nordgreen, T.; Liliedahl, T.; Sjöström, K. *Fuel* **2006**, *85*, 689.
(7) Furusawa, T.; Tsutsumi, A. *Appl. Catal., A* **2005**, *278*, 195.
(8) Tomishige, K.; Asadullah, M.; Kunimori, K. *Catal. Today* **2004**, *89*, 389.
(9) Simell, P. A.; Hirvensalo, E. K.; Smolander, V. T.; Krause, A. O. I. *Ind. Eng. Chem. Res.* **1999**, *38* (4), 1250.
(10) Gil, J.; Caballero, M. A.; Martin, J. A.; Aznar, M. P.; Corella, J. *Ind. Eng. Chem. Res.* **1999**, *38* (11), 4226.
(11) Rapagnà, S.; Jand, N.; Kiennemann, A.; Foscolo, P. U. *Biomass Bioenergy* **2000**, *19*, 187.
(12) Simell, P. A.; Leppälahti, J. P.; Bredenberg, J. B. *Fuel* **1992**, *71*, 211.
(13) Delgado, J.; Aznar, M. P.; Corella, J. *Ind. Eng. Chem. Res.* **1997**, *36*, 1535.
(14) Perez, P.; Aznar, P. M.; Caballero, M. A.; Gil, J.; Martin, J. A.; Corella, J. *Energy Fuels* **1997**, *11*, 1194.
(15) Simell, P. A.; Hepola, J. O.; Krause, A. O. I. *Fuel* **1997**, *76* (12), 1117.
(16) Taralas, G. *Ind. Eng. Chem. Res.* **1996**, *35* (*7*), 2121.
(17) Simell, P. A.; Hakala, N. A. K.; Haario, H. E.; Krause, A. O. I. *Ind. Eng. Chem. Res.* **1997**, *36* (1), 42.
(18) Narvaez, I.; Orio, A.; Aznar, M. P.; Corella, J. *Ind. Eng. Chem. Res.* **1996**, *35* (7), 2110.
(19) Hu, G.; Xu, S.; Li, S.; Xiao C.; Liu, S. *Fuel Process. Technol.* **2006**, *87*, *375*.
(20) Devi, L.; Ptasinski, K. J.; Janssen,F. J. J. G. *Fuel Process. Technol.* **2005**, *86*(*6*), 707.
(21) Devi, L.; Ptasinski, K. J.; Janssen, F. J. J. G. *Ind. Eng. Chem. Res.* **2005**, *44* (24), 9096.
(22) Devi, L.; Craje, M.; Thüne, P.; Ptasinski, K. J.; Janssen, F. J. J. G. *Appl. Catal., A* **2005**, *294* (1), 68.
(23) Juutilainen, S. J.; Simell, P. A.; Krause, A. O. I. *Appl. Catal., B* **2006**, *62* (1−2), 86.
(24) Bridgwater, A. V. *Chem. Eng. J.* **2003**, *91* (2−3), 87.

10.1021/cm0613511 CCC: $33.50
Published on Web 07/26/2006

preferred and most reliable system for large-scale applications. In particular, a catalyst has been designed to perform with the dual fluidized bed steam biomass gasifier (FICFB) developed by Hofbauer et al.[25] This type of reactor is divided in two zones for gasification and combustion, between which circulates a bed material acting as both a heat carrier and a catalyst. This permits us to produce a gas with a higher calorific value that is rich in H_2 and nearly free of N_2.

Previous works have demonstrated that natural olivine (iron and magnesium orthosilicate) can be an appropriate choice as bed material because of its hardness (similar to that of silica) and its catalytic activity in biomass steam gasification (comparable to that of dolomite).[11] The interest in the utilization of olivine as a catalyst has grown recently.[11,19−22] To enhance olivine performances and satisfy the above-mentioned requirements, Courson et al.[26] have previously developed a Ni−olivine catalyst; its performances have been proven on a laboratory scale in the reforming of methane[27] and toluene[28] as model compounds. The catalyst was then tested on a pilot-scale biomass gasification (FICFB gasifier) with steam by Pfeifer et al.,[29] which confirmed its suitability for steam gasification in a fluidized bed, although it was less interesting for tar destruction in air gasification, as shown by Corella et al.[30] The origin of the active phase, giving rise to its activity and stability (attrition and carbon-deposition resistance), was associated with strong Ni/olivine interactions developed during calcination; however, it was not very well characterized.

One of the keys to understanding the properties of the Ni/olivine system is the recently studied evolution of olivine alone in oxidizing−reducing conditions,[31] which showed the possibility of extracting free iron oxides from the olivine structure. For Ni/olivine catalysts in reducing conditions, this iron phase gives rise to the formation of the Ni−Fe alloys that are responsible for limiting carbon deposition.[32] It is also fundamental to understand the solid-state chemistry and the reducibility of the $NiO-Mg_2SiO_4$ system, because the reactions between those two phases induced by temperature can lead to the formation of the NiO−MgO solid solution[33] well-known for its anticoking properties.[34−36]

The aim of the present work is then to understand the origin and nature of the active phase issued from the Ni/olivine catalyst that is responsible for the excellent performance and stability during biomass steam gasification in the FICFB gasifier.[29] We have then followed the evolution of the Ni/olivine system after calcination and after reduction by means of X-ray diffraction, scanning electron microscopy, temperature-programmed reduction, and Mössbauer spectroscopy. Reactivity of the catalyst has been illustrated by methane and toluene steam reforming and carbon formation has been evaluated by temperature-programmed oxidation (TPO).

Experimental Section

Natural Olivine Support. Natural olivine was received from an Austrian mine (Magnolithe GmbH). It was delivered after calcination in air at 1600 °C for 4 h and crushing and sieving to obtain particles sizes between 400 and 600 μm. This material in fact contains $(Mg_{0.94}Fe_{0.06})_2SiO_4$ as the main phase, small quantities of $MgSiO_3$, and iron oxides (~3 wt % iron) $MgFe_2O_4$ and α-Fe_2O_3; this material is called the "initial olivine" and was used as the support for nickel. Its properties and evolution in oxidizing and reducing conditions are described elsewhere.[31]

Preparation of Ni/Olivine Catalyst. The Ni/olivine catalysts were prepared by wet impregnation of initial olivine with an aqueous solution of $Ni(NO_3)_2 \cdot 6H_2O$ to obtain a nickel content of 3.9 wt %. After water evaporation, the samples were dried overnight at 100 °C and then calcined under air for 4 h at different temperatures between 400 and 1400 °C with a heating rate of 3 °C min^{-1}. The real nickel content for all samples, verified by atomic absorption, was equal to the nominal value of 3.9 wt %.

Characterization Methods. Specific area measurements were carried out by using the BET method on the basis of the N_2 physisorption capacity at −196 °C (77 K) on a Coulter SA 3100 apparatus.

The crystalline phases contained in the samples and the structural modifications occurring after calcination and reduction were examined by powder X-ray diffraction (XRD) on a Siemens D500TT diffractometer using Cu Kα radiation ($\lambda = 1.5406$Å) with a step size of 0.02° 2θ and a step time of 20 s.

Scanning electron microscopy (SEM) was performed on a JEOL 6700 F microscope. The samples were first prepared for observing the surface morphology and measuring the compositional profiles in the bulk on cut grains. For this purpose, the samples were mounted in epoxy, cut in order to obtain planar sections, polished, and examined by SEM and X-ray microanalysis.

To quantify the amount of reducible iron and nickel, we have followed the reducibility of the catalyst by temperature-programmed reduction (TPR) performed on 200 mg of catalyst placed in a U-shaped quartz tube (6.6 mm ID). The reductive gas mixture ($H_2 = 0.12$ L h^{-1} and $Ar = 3$ L h^{-1}) passed through the reactor heated from room temperature to 950 °C with a slope of 15 °C min^{-1} and was then maintained at 950 °C until the end of H_2 consumption according to the baseline return. A thermal conductivity detector (TCD) was used for the quantitative determination of hydrogen consumption.

The ^{57}Fe Mössbauer spectra were recorded at −196 °C (77 K) using a spectrometer with a triangular waveform with a ^{57}Co source (50 mCi) dispersed in a rhodium matrix. From the obtained spectra, we determined the isomeric shifts in comparison with metallic iron standard at room temperature. To identify the different forms of iron present in the sample, we fitted the spectra with the MossFit computer program.

(25) Hofbauer, H.; Rauch, R.; Loeffler, G.; Kaiser, S.; Fercher, E.; Tremmel, H. *Six Years Experience with the FICFB−Gasification Process*, 12th European Conference and Technology Exhibition on Biomass for Energy, Industry and Climate Protection; Amsterdam, June 2002.
(26) Courson, C.; Petit, C.; Kiennemann, A.; Rapagna, S.; Foscolo, P. U.; Matera, D. PCT/FR01/01547 2001.
(27) Courson, C.; Udron, L.; Świerczyński, D.; Petit, C.; Kiennemann, A. *Çatal. Today* **2002**, *76*, 75.
(28) Świerczyński, D.; Courson, C.; Kiennemann, A. *Chem. Eng. Process.* **2006**, accepted.
(29) Pfeifer, C.; Rauch, R.; Hofbauer, H.; Świerczyński, D.; Courson, C.; Kiennemann, A. *Proceedings of the Science in Thermal and Chemical Biomass Conversion Conference*, Victoria, BC, Aug 30−Sept 2, 2004.
(30) Çorella, J.; Toledo, J. M.; Padilla R. *Energy Fuels* **2004**, *18*, 713.
(31) Świerczyński, D.; Courson, C.; Bedel, L.; Kiennemann, A.; Vilminot, S. *Chem. Mater.* **2006**, *18* (4), 897.
(32) Provendier, H.; Petit, C.; Kiennemann, A. *C. R. Acad. Sci., Ser. IIC: Chim.* **2001**, *4*, 57.
(33) Shirane, Y.; Morinaga, K.; Yanagase, T. *Int. J. Miner. Process.* **1987**, *19*, 253.
(34) Yamazaki, O.; Tomishige, K.; Fujimoto, K. *Appl. Catal., A* **1996**, *136*, 49.
(35) Tomishige, K.; Chen, Y. G.; Fujimoto, K. *J. Catal.* **1999**, *181*, 91
(36) Hu, Y. H.; Ruckenstein, E. *Catal. Rev. Sci. Eng.* **2002**, *44* (3), 423.

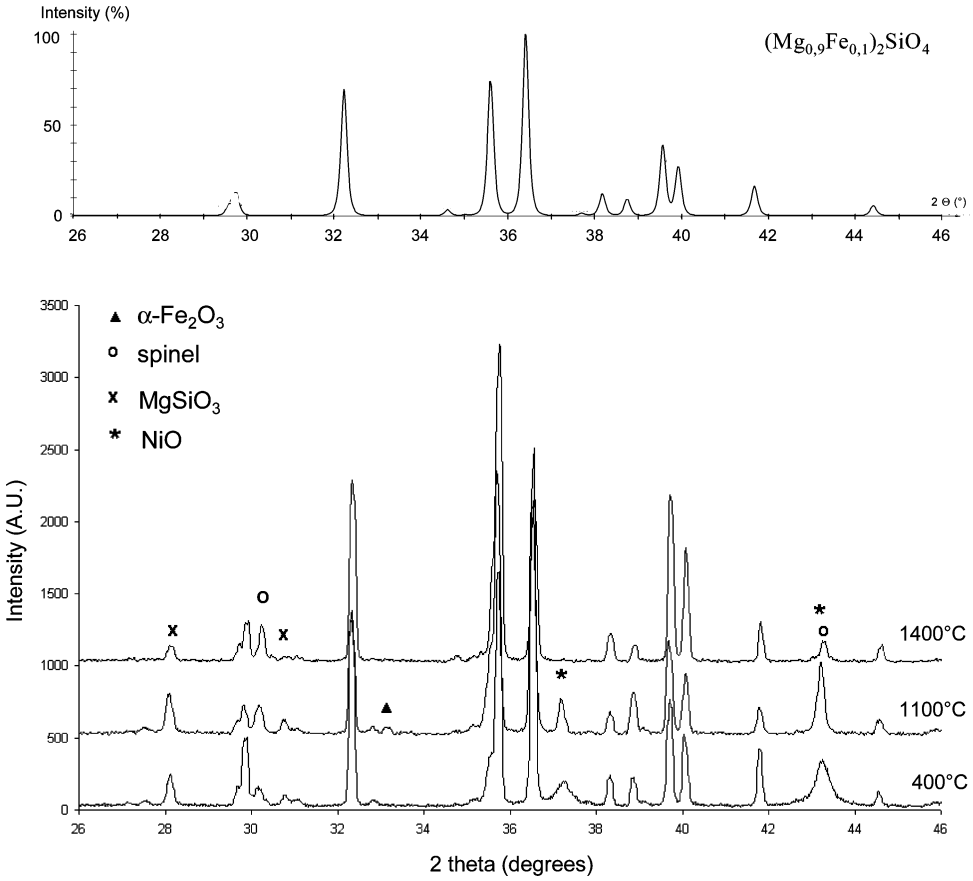

Figure 1. Diffractograms of 3.9%Ni/olivine catalysts calcined at 400, 1100, and 1400 °C. The reflections without indications correspond to the olivine phase; the theoretical diffractogram of $(Mg_{0.9}Fe_{0.1})_2SiO_4$ is on top.

The amount of carbon deposited on the catalyst during the reactivity tests can be determined by the quantification of the oxidation products (CO_2) observed by temperature-programmed oxidation (TPO). This analysis was performed on 25 mg of catalyst placed in a U-shaped quartz tube (6.6 mm ID). The oxidizing gas mixture (O_2 = 5 mL min^{-1} and He = 45 mL min^{-1}) passed through the reactor that was heated from room temperature to 970 °C with a slope of 15 °C min^{-1}.

Catalytic Tests. The catalytic activity of the Ni/olivine catalyst was studied in the steam reforming of methane and toluene as the tar model compound in a fixed bed reactor with the experimental bench previously described.[27,28] For methane steam reforming, the operating conditions were as follows: total feed flow rate = 3 NL h^{-1}; weight of catalyst = 200 mg; H_2:CO:CO_2:CH_4:N_2 (vol %) inlet gas composition = 34:26:18:9:13, on the basis of the gas composition produced by the biomass steam gasification in the FICFB gasifier.[29] For toluene steam reforming, the catalyst (200 mg) was activated at 750 °C for 30 min before the catalytic test under a total feed flow rate of 3 NL h^{-1} with the following composition: 87.7% argon, 11.6% water, and 0.7% toluene.

Results and Discussion

Influence of Calcination Temperature on the Evolution of Ni/Olivine Systems. *BET Surface Area.* The specific surface area of the initial olivine is very low (<1 m^2 g^{-1}) because of its initial sintering (melting point of approximately 1760 °C); this olivine can be considered as being nonporous. The surface area of Ni/olivine catalysts can then be mainly attributed to the presence of a NiO shell enveloping the olivine grain. The diminution of the specific surface area from 3.7 m^2 g^{-1} (calcined at 400 °C) to 1.7 m^2 g^{-1} (calcined at 1100 °C) and <1 m^2 g^{-1} (calcined at 1400 °C) can be observed and better understood after XRD data analysis.

X-ray Diffraction. X-ray diffraction was used for the identification of the crystalline phases and to follow the structural modifications occurring upon thermal treatments. The diffractograms of Ni/olivine calcined between 400 and 1400 °C (Figure 1) permit us to distinguish between two temperature ranges (400−1100 °C and 1100−1400 °C) associated with different phase modifications. The reflections that are not identified on the graph correspond to the olivine phase indicated on the top. The secondary phases resulting from the olivine oxidation are iron oxides α-Fe_2O_3, spinel phase ($MgFe_2O_4$), and enstatite ($MgSiO_3$).

For the calcination temperatures between 400 and 1100 °C, in addition to the above-mentioned phases, the NiO phase formed by decomposition of nitrates can be observed. Narrowing of the principal reflection of NiO (2θ = 43.2°) for the system calcined at 1100 °C in comparison to that calcined at 400 °C indicates an increase in the particle size during calcination (between 400 and 1100 °C), confirmed by diminution of the specific surface area. Additionally, an increase in the contribution of the iron oxide phases and presence of enstatite phase $MgSiO_3$ can be observed that is similar to that in olivine alone calcined in the same temperature range.[31]

The intensity of the principal reflection of NiO diminishes when the calcination temperature increases from 1100 to 1400 °C, indicating that Ni is progressively integrated in

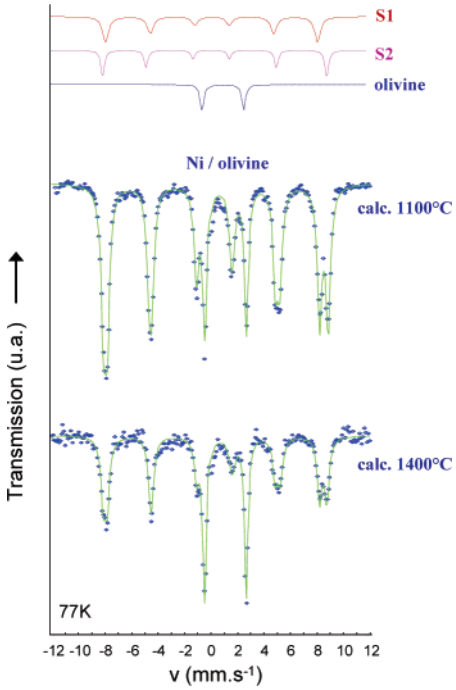

Figure 2. ^{57}Fe Mossbauer spectra at −196 °C (77 K) of Ni/olivine calcined at 1100 and 1400 °C; the subspectra of the three components are indicated at the top.

another structure (olivine). For the calcination temperature of 1400 °C, the diminishment of the $MgSiO_3$ phase and disappearance of the main reflections of α-Fe_2O_3 and NiO ($2\theta = 43.25°$ and 37.28°) can be noticed. Let us recall here that the surface area of this system is similar to that of olivine and permits us to suppose that the NiO shell has disappeared. At the same time, the rejection of iron oxide from the olivine structure can be seen by the increase in the reflection at $2\theta = 30.25$ and 35.61° (spinel phase), which is superimposed over the NiO main reflection.

In the case of the Ni/olivine catalyst, the increase in the amount of iron oxide phases observed by XRD for calcination temperatures between 1100 and 1400 °C can be explained as either a phenomenon related only to olivine oxidation (hypothesis I) associated with iron extraction (thermal stability of the olivine phase as a function of iron content)[31] or a result of exchange between iron and nickel in the olivine structure (hypothesis II). If the second hypothesis is true, we should observe a lower iron content in the olivine structure for the Ni/olivine catalyst than for olivine alone calcined at the same temperature. To check which hypothesis is true and to supply additional evidence, we examined the samples calcined at 1100 and 1400 °C by Mössbauer spectroscopy.

Mössbauer Spectroscopy. The ^{57}Fe Mossbauer spectra for those Ni/olivine samples are shown in Figure 2. Similar to the case of olivine alone,[31] the theoretical spectrum of Ni/olivine catalyst can be described as a sum of three subspectra. The theoretical Mössbauer spectra for Ni/olivine calcined at 1100 and 1400 °C show good accordance with the experimental data, as shown in Figure 2.

The parameters of the three subspectra for Ni/olivine calcined at 1100 and 1400 °C are given in Table 1. The quadrupole doublet present in the Mössbauer spectra with

Table 1. Mössbauer Parameters of Components Present in Ni/Olivine Calcined at 1100 and 1400 °C[a]

	$T_{calcination}$ (°C)	
	1100	1400
Doublet Fe^{2+} (olivine)		
δ (mm s^{-1})	1.13	1.12
Δ (mm s^{-1})	3.06	3.06
H (kG)	0	0
R (%)	19	33
Sextet 1 Fe^{3+}		
δ (mm s^{-1})	0.24	0.23
Δ (mm s^{-1})	−0.01	−0.01
H (kG)	495	495
R (%)	39	32
Sextet 2 Fe^{3+}		
δ (mm s^{-1})	0.36	0.36
Δ (mm s^{-1})	0.09	−0.03
H (kG)	524	521
R (%)	42	35

[a] δ, isomer shift related to metallic iron; Δ, quadrupole splitting; H, hyperfine field; R, relative area.

Table 2. Distribution of Iron in Different Phases Obtained from Mössbauer Spectroscopy for Olivine and Ni/Olivine Calcined at 1100 and 1400 °C

	calcined at 1100 °C		calcined at 1400 °C	
iron type	olivine	Ni/olivine	olivine	Ni/olivine
Fe^{3+} (S1)	29	39	41	32
Fe^{3+} (S2)	54	42	39	35
Fe^{2+} (olivine)	17	19	20	33

an isomer shift of ∼1.12 mm s^{-1} and quadrupole splitting of ∼3.06 mm s^{-1} is due to Fe^{2+} ions in the olivine structure.[37] The two other components are two magnetic sextets (S1 and S2) with isomer shift values of 0.26 and 0.36 mm s^{-1}, which are characteristic of Fe^{3+} ions.[38,39] They can be attributed to the iron in the form of α-Fe_2O_3 and spinel phase ($MgFe_2O_4$).

Table 2 presents a comparison of iron distribution in different phases for olivine[31] and Ni/olivine calcined at 1100 and 1400 °C.

Taking into consideration the amount of iron in the olivine lattice, we can observe nearly the same values for olivine and Ni/olivine calcined at 1100 °C. For the samples calcined at 1400 °C, we find even more iron present in the olivine structure for Ni/olivine than for olivine alone, which could be explained by the presence of a nickel oxide layer on the olivine surface that inhibits the diffusion and access of oxygen to the surface of olivine and finally limits the oxidation of Fe^{2+} in olivine. It also cannot be excluded that the integration of nickel in the olivine structure and formation of the $(Mg, Fe, Ni)_2SiO_4$ system changes the thermodynamically determined equilibrium between the amount of iron in the olivine structure and in the form of oxides.[40]

Considering the results, we must discard hypothesis II, which is that an exchange between iron and nickel occurs. It means that nickel integration in the olivine structure after calcination at 1400 °C must be due to an exchange between nickel and magnesium according to the following reaction

(37) Meyer, M.; Rüffler, R. *Hyperfine Interact.* **2002**, *141/142*, 351.
(38) Imelik, B.; Védrine, J. C. *Les Techniques Physiques d'Étude des Catalyseurs*; Technip: Paris, 1998.
(39) Greenwood, N. N.; Gibb, T. C. *Mössbauer Spectroscopy;* Chapman Hall: London, 1971.
(40) Nitzan, U. *J. Geophys. Res*. **1974**, *79*, 706.

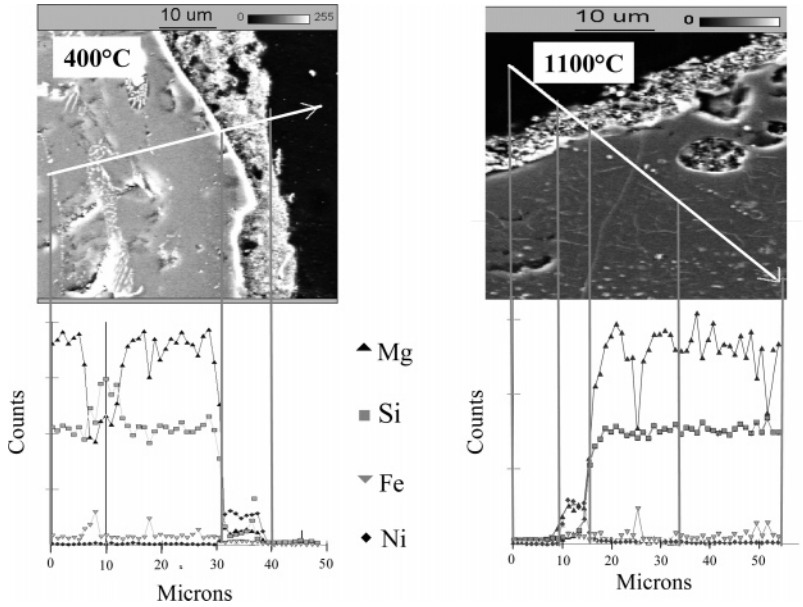

Figure 3. SEM micrographs and microanalysis on cut grains of Ni/olivine calcined at 400 and 1100 °C.

(for simplicity, the Fe present in olivine is not indicated)

$$Mg_2SiO_4 + 2xNiO \rightarrow (Mg_{1-x}Ni_x)_2SiO_4 + 2xMgO$$

The knowledge of the evolution of Fe^{2+}-, Fe^{3+}-, and Ni^{2+}-containing phases with calcination temperature acquired with XRD and Mössbauer will serve as a basis for better understanding of the reducibility of Ni/olivine systems.

Influence of Calcination Temperature on the Reducibility of Ni/Olivine Systems. The reduced nickel is well-known to be the active phase of nickel catalysts in hydrocarbons and tar reforming. Using nickel oxide deposited on olivine requires preliminary or in situ reduction in order to obtain the active catalyst. As the working conditions of the catalyst are generally reducing (800 °C, presence of hydrocarbons, CO, and H_2), studies of the catalyst reducibility permit us to predict its evolution during the catalytic tests by giving valuable information: at which temperature nickel species can be reduced as well as the quantity and composition of the metallic phase. For this reason, we have studied the reducibility of Ni/olivine catalysts by temperature-programmed reduction (TPR). The reduced systems have then been examined by Mössbauer spectroscopy and X-ray diffraction.

The profiles of hydrogen consumption as a function of temperature for Ni/olivine catalysts calcined at different temperatures were previously obtained by temperature-programmed reduction.[41] For all the samples, the zone of hydrogen consumption between 450 and 800 °C (with a maximum at ca. 660 °C) is due mostly to the reduction of free iron oxides resulting from olivine oxidation and, to a small extent, reduction of nickel species. The intensity of this zone increases with calcination temperature similar to that for olivine alone.[31]

After calcination at 400 °C, nickel oxide is reduced at ca. 400 °C, which means that it is just deposited on the olivine surface with a weak interaction type. The shift in the temperature corresponding to the maximum in hydrogen consumption from 400 to 910 °C is observed for the systems calcined at 400 and 1100 °C. It can correspond to the reduction of Ni^{2+} included in a structure other than NiO; however, no new phase was observed by XRD. This high reduction temperature is associated with a strong nickel-support interaction. The presence of theses "grafted" nickel species could be then explained by the formation of a new phase that either is amorphous or has the same structure as NiO or olivine and is thus nondistinguishable by XRD. According to the TPR results, the presence of the reduction peak at 910 °C supports the hypothesis of a NiO−MgO solid solution forming from the interaction between NiO and the MgO phase rejected after calcination at 1100 °C.[42]

For the catalyst calcined at 1400 °C, the disappearance of the reduction zone with a maximum at 910 °C is observed and can be explained by integration of nickel in the olivine structure, which is not reducible under the TPR conditions. To differentiate those three types of Ni−olivine interactions, we examined the three samples calcined at 400, 1100, and 1400 °C by scanning electron microscopy (SEM) coupled with X-ray microanalysis; the analyses were carried out on grain cuts.

Study of Interactions between NiO and Olivine. *Scanning Electron Microscopy.* The SEM micrographs in Figures 3 and 4 show the catalyst grain border with a layer (shell) of oxide (5−20 μm) on the olivine surface. This layer is composed of only NiO for the sample calcined at 400 °C. After calcination at 1100 °C, EDX analysis reveals the presence of NiO and MgO in a 1/1 Ni/Mg ratio that is also an argument for the formation of a NiO−MgO solid-solution phase.

The formation of this phase can be explained by a magnesium−nickel exchange between the olivine and the

(41) Świerczyński, D.; Courson, C.; Guille, J.; Kiennemann, A. *J. Phys. IV* **2004**, *118*, 385.

(42) Serra, M.; Salagre, P.; Cesteros, Y.; Medina, F.; Sueiras, J. E. *Solid State Ionics* **2000**, *134*, 229.

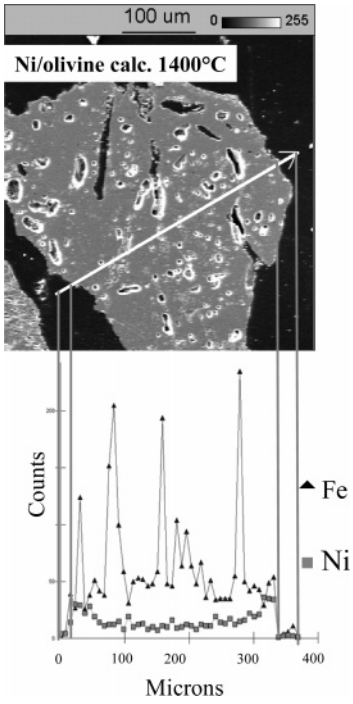

Figure 4. SEM micrograph and microanalysis on cut grain of Ni/olivine calcined at 1400 °C.

NiO phases, resulting in strong nickel−olivine interactions observed by temperature-programmed reduction (TPR). It should be noted, however, that it was not possible to identify this phase by XRD, as the diffraction patterns of NiO and MgO are very close to each other;[42] the simultaneous presence of both phases gives rise to widening reflections and makes clear distinction impossible.

Calcination at higher temperatures leads to the graduate integration of nickel into the olivine structure, accomplished at 1400 °C, as observed in Figure 4 by the diffusion profile of nickel in the bulk of the olivine grain. The concentration of nickel is elevated in the first 50 μm from the grain surface and then remains constant in the whole depth of the grain.

SEM on grain cuts and EDX analysis confirm the three states of interaction between nickel oxide and olivine support, free NiO, NiO−MgO solid solution, and nickel integrated into olivine, and permits us to propose a mechanism of reaction taking place between NiO and olivine during the calcination.

According to Shirane et al.,[33] who studied the solid-state reactions in the NiO−MgO−SiO_2 system, the reaction between NiO and olivine can be described by the following equation

$$Mg_2SiO_4 + n\text{NiO} \rightarrow (Mg_{1-y}Ni_y)_2SiO_4 + n(Ni_{1-2y/n}Mg_{2y/n})\text{O where } n \leq 2$$

The rate of this reaction (dy/dt) depends strongly on the temperature; as the activation energy for diffusion in silicates is high, the diffusivity increases rapidly with temperature. Generally, an increase in temperature of 100 °C leads to an increase in the diffusion coefficient of about 1 order of magnitude.[43] The authors have shown that for a mixture of

(43) Dereń, J.; Haber, J.; Pampuch, R. *Chemia Ciał Stalego*; PWN: Warsaw, 1975.

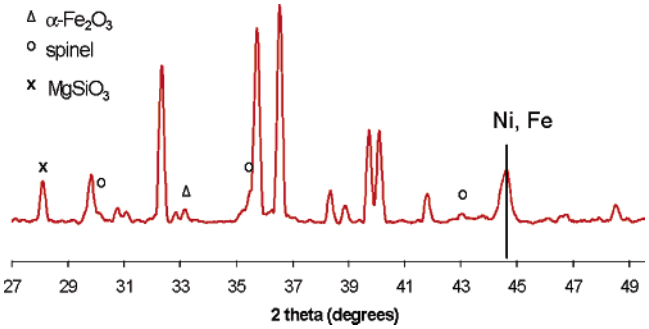

Figure 5. Diffractogram of Ni/olivine calcined at 1100 °C after TPR.

$Mg_2SiO_4 + {}^1/_2\text{NiO}$, after 1 h of reaction, more than 70% of the nickel was exchanged at 1400 °C, but only 5% of nickel at 1200 °C. For the Ni/olivine system in the range of calcination temperatures between 400 and 1100 °C, the reaction between NiO and olivine is slow and limited to only the olivine grain surface, which leads to the formation of the NiO−MgO solid solution at 1100 °C. Calcination at temperatures higher than 1100 °C leads to the graduate diffusion of nickel in the bulk of the olivine grain, leaving MgO, which can then react with enstatite according to:

$\text{MgO} + \text{MgSiO}_3 \rightarrow Mg_2SiO_4$ which explains the absence of MgO and diminishing of $MgSiO_3$ as observed by XRD for systems calcined between 1100 and 1400 °C. It should be noted here that the reaction between NiO and $MgSiO_3$ with the formation of $NiMgSiO_4$ could also contribute, to some extent, to the diminishing of the $MgSiO_3$ phase.

Characterization of the Phases Observed after Reduction of Ni/Olivine Calcined at 1100 °C. *XRD.* After total reduction of the Ni/olivine catalyst, XRD shows (Figure 5) that the main olivine phase is unchanged; the peak intensities of the spinel phase and α-Fe_2O_3 decrease and a new peak appears at 44.6° (2θ) that can be attributed to the main reflection of metallic nickel or nickel−iron alloy (Ni, Fe), kamacite; however, XRD does not permit us to differentiate those phases.[44,45]

Mössbauer Spectroscopy. To verify which are the iron containing phases after reduction, we examined the reduced catalyst (Ni/olivine calcined at 1100 °C) by Mössbauer spectroscopy.

The Mössbauer spectrum of Ni/olivine calcined at 1100 °C after TPR is presented in Figure 6.

The parameters of the theoretical subspectra are given in Table 3. In addition to the three components present in the nonreduced sample, we find the presence of a new sextet. Its hyperfine parameters are typical for kamacite, an α-Fe−Ni alloy.[46−48] Because of the presence of nickel, the isomer shift is slightly positive relative to that of α-iron and the hyperfine field is larger than that of iron.

Table 4 shows the comparison of the distribution of iron in different phases obtained from Mössbauer spectroscopy for Ni/olivine calcined at 1100 °C before and after TPR.

The iron-containing phases present in reduced Ni/olivine are the same as in the reduced olivine.[31] Iron in the form of

(44) Powder diffraction file for Ni, 4-0850; International Center for Diffraction Data: Newtown Sqaure, PA.
(45) Powder diffraction file for Ni−Fe, 37-474; International Center for Diffraction Data: Newtown Square, PA.

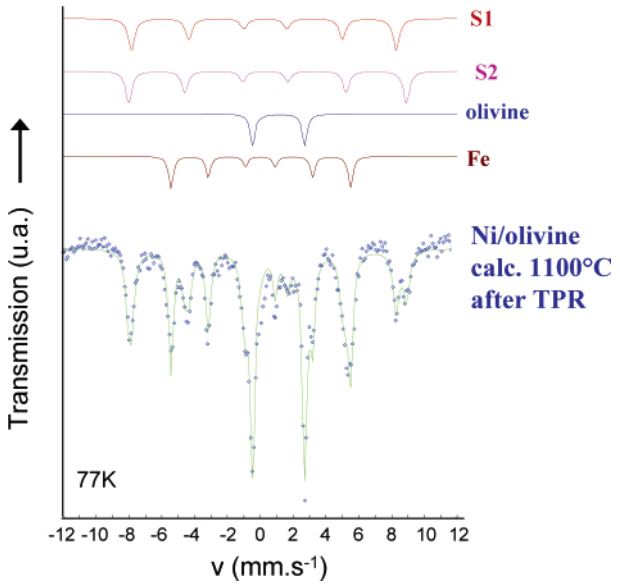

Figure 6. ^{57}Fe Mossbauer spectra at −196 °C (77 K) of Ni/olivine calcined at 1100 °C after TPR; the subspectra of the four components are indicated at the top.

Table 3. Mössbauer Parameters of Components Present in Ni/Olivine Calcined at 1100 °C after TPR[a]

	δ (mm s^{-1})	Δ (mm s^{-1})	H (kG)	R (%)
doublet Fe^{2+} (olivine)	1.14	3.07	0	31
sextuplet 1 (Fe^{3+})	0.28	−0.10	498	22
sextuplet 2 (Fe^{3+})	0.38	0.14	522	16
sextuplet 3 α-Ni−Fe	0.02	0	337	31

[a] δ, isomer shift related to metallic iron; Δ, quadrupole splitting; H, hyperfine field; R, relative area.

Table 4. Distribution of Iron in Different Phases Obtained from Mössbauer Spectroscopy for Ni/Olivine Calcined at 1100 °C after TPR

iron type	Ni/olivine calcined at 1100 °C	Ni/olivine calcined at 1100 °C after TPR	%Fe^{3+} reduced	
Fe^{3+} (S1)	39	22	17	
Fe^{3+} (S2)	42	16	26	
total Fe^{3+} (S1 + S2)	81		43	
Fe^{2+} (olivine)	19	31		12/43 $Fe^{3+} \rightarrow Fe^{2+}$
Fe^{0} (α-Ni−Fe)		31		31/43 $Fe^{3+} \rightarrow Fe^{0}$

iron oxides (Fe^{3+}) represents 81% of the total iron present in the olivine. Under the TPR conditions, 53% of iron oxides were reduced, representing 43% of the iron present in olivine. It is reduced mostly (31%) to metallic iron, which forms an alloy with nickel, and the remaining 12% is reduced to Fe^{2+}, which reintegrates with the olivine structure.

This study permitted us to confirm the presence of nickel−iron alloy in the sample after TPR and to quantify that this phase formed with the greater part of the reduced iron. This phase formation will also be formed under reaction conditions and then ensure a carbon deposit resistance of the Ni/olivine catalyst.

Catalytic Efficiency of Ni/Olivine Catalyst in Methane and Toluene Steam Reforming. To illustrate the efficiency of the Ni/olivine catalyst, we present a summary of catalytic results.

Steam Reforming of Methane. This study in a fixed bed reactor has indicated that the composition of the gas issued from the biomass steam gasification in the FICFB gasifier

Table 5. Influence of the Ni/Olivine Presence on the Dry Gas Composition Similar to that Issued from the Biomass Steam Gasification in the FICFB Gasifier (water content = 35 vol %, T = 800 °C)

dry gas components	dry gas composition[a] (vol %)	after reactivity with Ni/olivine catalyst
H_2	34	46
CO	26	28
CO_2	18	15
CH_4	9	1
N_2	13	10

[a] Similar to that issued from the biomass steam gasification in the FICFB gasifier.[29]

can be improved by the Ni/olivine presence. An increase in H_2 production (Table 5) associated with a decrease in methane content was particularly observed without deactivation of the catalyst during 7 h of testing for a water content of 35 vol % in the inlet gas.

These results are in good agreement with those obtained by Pfeifer et all.[29] in steam gasification of biomass in the FICFB gasifier.

Steam Reforming of Toluene. Toluene was used as a tar model compound because it represents a stable aromatic structure apparent in tar formed with high-temperature processes and is one of the major tar species.[49] For a better understanding of tar destruction, toluene steam reforming was chosen as a model reaction. The conversion of toluene on the Ni/olivine catalyst was complete at a reaction temperature higher than 650 °C and the product gases were only H_2, CO, and CO_2. These results have to be compared with those obtained with olivine alone. In this case, the toluene conversion was about 37% at 850 °C, and the product gas contained significantly heavier polyaromatics (14%), benzene (∼6%), and methane (2%) formed additionally from CO, CO_2, and H_2. The efficiency of the Ni/olivine catalyst can also be observed by its resistance of carbon formation. In fact, after steam reforming of toluene at 850 °C, the amount of carbon formed on the catalyst is less than 3 μg/(g_{cat} h C_{conv}) compared to 10 μg/(g_{cat} h C_{conv}) on olivine alone in the same conditions.

Conclusions

In conclusion, the present study has permitted us to explain the mechanism of formation and the nature of the active phase of the Ni/olivine catalyst, making it possible to connect its structure with activity and stability during reforming of model hydrocarbons as well as biomass steam gasification in the FICFB gasifier.[29] The catalyst that results from subsequent calcination and reduction of the precursor obtained by the impregnation of natural olivine with nickel nitrate can be described as a Ni−Fe/MgO/olivine system, where olivine is initially a system containing $(Mg_{0.94}Fe_{0.06})_2SiO_4$ as the main phase and small quantities of $MgSiO_3$ and iron oxides (∼3 wt % iron) $MgFe_2O_4$ and α-Fe_2O_3. Two phenomena contribute to the formation of this active system. The first one is a solid-state reaction between NiO and

(46) Fultz, B.; Morris, J. W. *J. Phys. Rev.* **1986**, *B34*, 4480.
(47) Vincze, I.; Gruner, G. *Phys. Rev. Lett.* **1972**, *28*, 178.
(48) Vincze, I.; Campbell, I. A.; Meyer, A. J. *Solid State Commun.* **1974**, *15*, 1495.

olivine, which, during calcination at 1100 °C, leads to the formation of NiO−MgO solid solution on the olivine surface, responsible for the high resistance to carbon deposition during reformation reactions. The second one is the oxidation of the iron-bearing olivine induced by calcination and leading to the formation of iron oxides. Under reducing conditions, theses phases lead to the formation of Ni−Fe alloys known for having a beneficial effect on increasing carbon-deposition resistance. The preparation method used for this catalytic system presents the advantages of low cost (water as solvent), simplicity, and reproducibility on the large scale and can be considered to be of interest for industrial applications, as demonstrated in this paper, for example, in methane and toluene steam reforming and also in a FICFB demonstration unit.[29]

Acknowledgment. This work was carried out under EC Project NNE5-2000-00212 (Contract ENK5-CT2000-00314). We thank the European Commission for its financial support.

CM0613511

(49) Milne, T. A.; Abatzoglou, N.; Evans, R. J. *Biomass Gasification "Tars": Their Nature, Formation and Conversion*; Report NREL/TP-570-25357; National Renewable Energy Laboratory: Golden, CO, 1998.